J. Mt. Sci. (2011) 8: 619–628
DOI: 10.1007/s11629-011-2129-0

Numerical Investigation on the Initiation Mechanism of Debris-Flow under Rainfall

LU Xiaobing[1]*, YE Tianli[1], CUI Peng[2], HU Kaiheng[2], CHEN Xiaoqing[2]

1 Institute of Mechanics, Chinese Academy of Science, Beijing, 100084, China;

2 Institute of Mountain Hazards and Environment, Chinese Academy of Science, Chengdu, 610041, China

** Corresponding author, e-mail: xblu@imech.ac.cn*

Abstract: Rainfall is an important factor to trigger the debris flow. Numerical simulation on the responses of slopes and the initiation of debris flow under rainfall was processed by using the software FLAC2D based on the soil parameters in Weijia Gully, Beichuan County, Sichuan Province, China. The effects of the slope angle, rainfall intensity, soil parameters on the developments of the stress and pore pressure and deformation of the slope were studied. It indicates that large displacements of the slope are mainly located near the slope toe. With the increase of the rainfall intensity the stability of the slope decreases and so the debris-flow is easy to occur.

Keywords: Debris-flow; Initiation mechanism; Rainfall; Numerical simulation

Introduction

Landslides and debris flows, distributing broadly in nature, restrict the economic development and threaten the safety of towns, villages, traffic and dams. 90% to 95% of these hazards are caused by rainfall (Chen et al. 2006). A mass of debris flows and landslides were triggered by rainfall after the May 12th earthquake in 2008. Therefore, the forecast for landslide and debris flow is an important mission in the earthquake affected area.

Although many studies on the forecast of landslide and debris flow have been carried out (Cui et al. 2000; Aleotro 2004), there is still not a precise method which can be applied broadly because of the limited understanding on the initiation mechanism. Experiments and in-situ measurements were used in studying the initiation of debris flow in the previous studies (Cui 1992; Iverson et al. 1997; Cui et al. 2007), while numerical simulations were few used. However, numerical simulations can analyze the distribution of stresses, displacement and pore pressure in a slope which can not be obtained fully in experiments. Furthermore, numerical simulations can investigate some special cases easily. For an example, the erosion and the re-deposition of fine grains which play an important role in the initiation of debris flow can be detailed simulated easily by using numerical methods (Cui et al. 2009; Lu et al. 2006; Lu and Cui 2010; Lu et al. 2010) while difficultly by using experiments.

Seepage and surface flow during a rainstorm can obviously change the distribution of pore pressure and the mechanical properties of a slope. These changes will alter the stresses and the deformation of a slope. Conversely, stress and deformation changes can alter the seepage process because the hydraulic properties such as the porosity, permeability and water storage capacity were affected by the changes in stresses. Hence the seepage and stress-deformation problems are strongly linked (Zhang et al. 2005; Wu et al. 2009). Duration is an important parameter with which to

Received: 29 January 2011
Accepted: 20 April 2011

forecast the initiation of debris flow, particularly for a real-time monitoring system (Chen et al. 2005).

In the above viewpoints, the objective of this paper is to numerically investigate the responses of stresses, pore pressure, deformation and duration to yield enough water for debris flow triggering.

1 Properties of In-Situ Soils

The in-situ soils in the Weijia Gully in Beichuan County in China were taken for experiments. The grain sizes of the soils are widely distributed as shown in Figure 1. The dry density is 1579 kg/m^3 and the saturation density is 2000 kg/m^3.

The static triaxial apparatus was used to determine the parameters of constitutive relation. There is no peak in the curves of axial strain and deviatoric stress (Figure 2). That means, the failure of this kind of soil is plastic, so the stress at axial strain 20% is taken as the failure value (If the soil is brittle, the stress at the peak is taken as the failure value). The internal friction angle and the cohesion can be obtained by Mohr circles as 22.2° and 6 *kPa*, respectively. The initial Yang's modulus is 1×10^8 MPa.

2 Numerical Simulation

2.1 Numerical Model

Business software FLAC2D5.0 was used to simulate the responses of a slope under rainfall. The parameters used in numerical simulations were the same with that in the model experiments (Ye 2011). The bottom was vertically fixed, the top was free, the height of the slope was 20 cm, the slope angles were 27°, 30° and 33°， respectively. The other boundaries were all normally fixed (Figure 3). The Mohr-Column model was used to describe the mechanical behavior of the slope. The seepage of two phases (pore air and pore water) was considered to obey the Darcy Law. The mechanical parameters are shown in table 1.

The seepage equations for the pore water and the pore air are shown in the following:

$$q_{ij}^{w} = -k_{ij}^{w} k_{r}^{w} \frac{\partial}{\partial x_j}\left(P_w - \rho_w g_k x_k\right) \quad (1)$$

$$q_{ij}^{g} = -k_{ij}^{g} k_{r}^{g} \frac{\partial}{\partial x_j}\left(P_g - \rho_g g_k x_k\right) \quad (2)$$

The strength criterion is:

$$\tau^{\max} = (\sigma - P_a)\tan\phi + S_w(P_a - P_w)\tan\phi + C \quad (3)$$

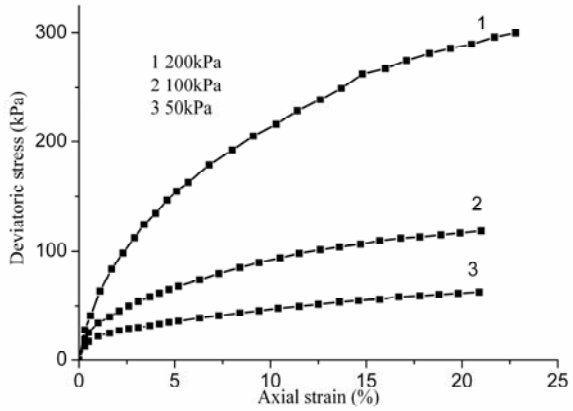

Figure 2 Axial strain versus deviatoric stress

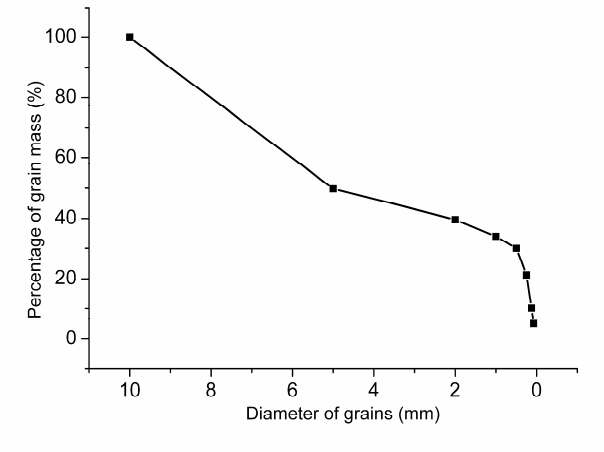

Figure 1 Grain series curves of Beichuan County soil

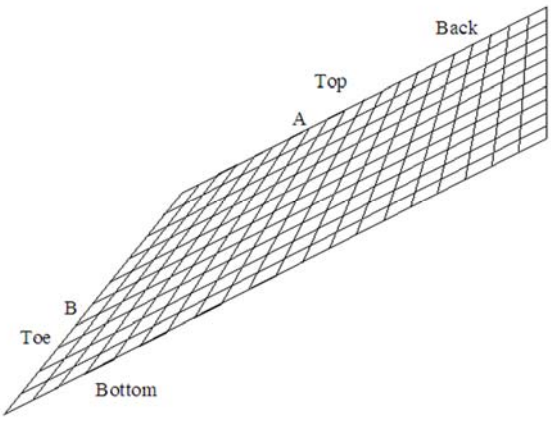

Figure 3 Network for numerical simulation

Table 1 Mechanical parameters of the slope

Dry density (kg/m^3)	Permeability (cm/s)	Cubic modulus (GPa)	Shear modulus (GPa)	Cohesion (kPa)	Internal friction angle (°)
2000	1.0×10^{-4}	0.8	0.6	6	22.2

Table 2 Rainfall intensity adopted in the numerical simulation

Slope angle (°)	Rainfall intensity (mm/h)				
27	36	72	108	144	180
30	36	72	108	144	180
33	36	72	108	144	180

The capillary force is satisfied the following equation:

$$P_c = P_g - P_w \tag{4}$$

and

$$P_c = P_0\left[S_e^{-1/a} - 1\right]^{1-a} \tag{5}$$

The relative permeability of the pore water is:

$$k_r^w = S_e^b\left[1 - \left(1 - S_e^{1/a}\right)^a\right]^2 \tag{6}$$

The relative permeability of the pore gas is:

$$k_r^g = \left(1 - S_e^b\right)^c\left(1 - S_e^{1/a}\right)^{2a} \tag{7}$$

and

$$S_e = \frac{S_w - S_r^w}{1 - S_r^w} \tag{8}$$

in which q_{ij}^w, q_{ij}^g are flow rates of water and air, k_{ij}^w the saturated permeability, k_r^w the relative permeability of water, k_r^g the relative permeability of air, P_w the pore water pressure, P_g pore gas pressure, ρ_w density of water, ρ_g density of gas, g_k, x_k the gravity acceleration and position, when their directions are different, their product equals zero, τ^{max} the strength, σ the total stress, S_e the effective saturation of pore water, S_w saturation of water, ϕ internal friction angle, C cohesion, S_r^w residual saturation of water, a, b are constant coefficients.

2.2 Scheme of the Numerical Simulation

The rainfall intensity, slope angle, density and strength and permeability of the soil were mainly considered in the numerical simulation. The rainfall intensity ranged from 36 mm/h to 180 mm/h (Table 2). The network of the slope for numerical simulations is shown in Figure 3. Points A and B are chosen as the character points and the data at these two points are used in the analysis.

2.3 Numerical Results and Analysis

The results simulated with the parameters of rainfall intensity 36 mm/h, slope angle 27°, and rain duration 100s are used for the discussion in this section. The maximum saturation degree of water is located near the surface of the slope (Figures 4, 5). The reason is that the permeability decreases with the increase of the water saturation degree, so the water is blocked at the locations near the surface with the seepage. The maximum pore pressure is also near the surface of the slope corresponding to the water saturation degree

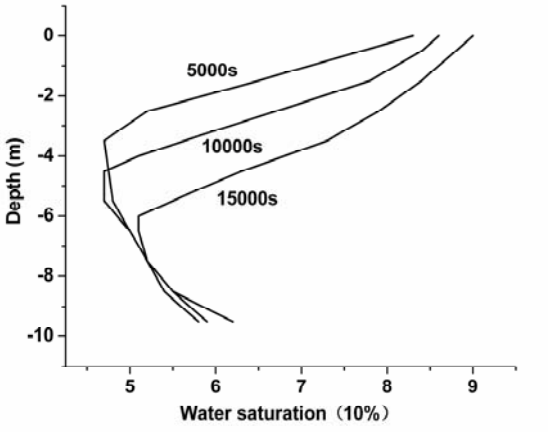

Figure 4 Development of saturation degree with depth under different rainfall intensity

(Figure 6). The horizontal displacements increase with time and develop fast with the increase of rainfall intensity. It is shown also that there is an inflextion at the displacements vs time curves. In other words, the developments of the displacements are catastrophic (Figures 7, 8). The maximum velocity of the soils' movement is located near the toe and formed a curve as a potential

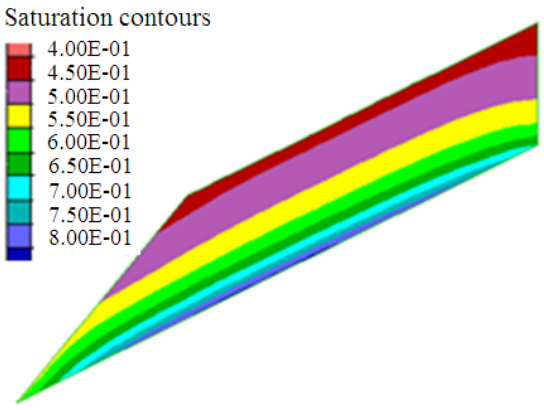

Figure 5 Distribution of saturation degree at 600s

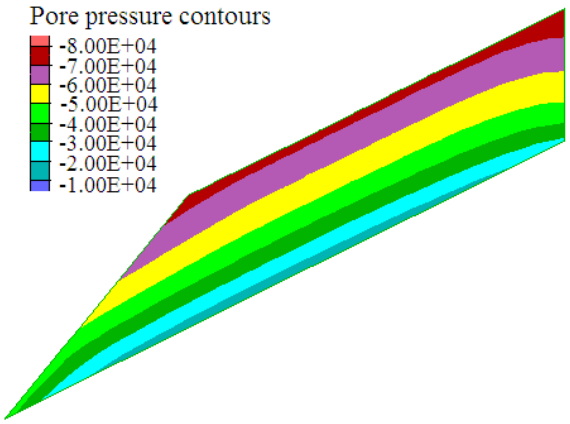

Figure 6 Distribution of pore pressure at 600s

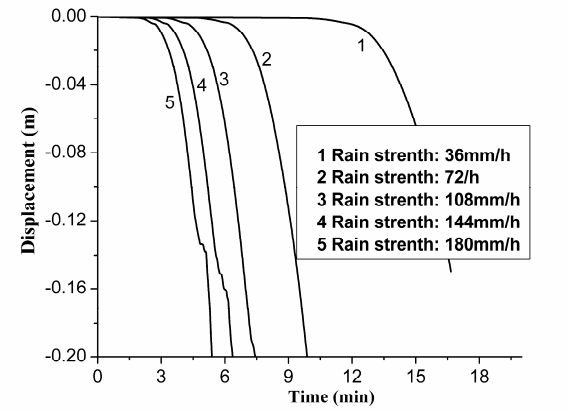

Figure 7 Development of the horizontal displacement at point A under different rainfall intensities

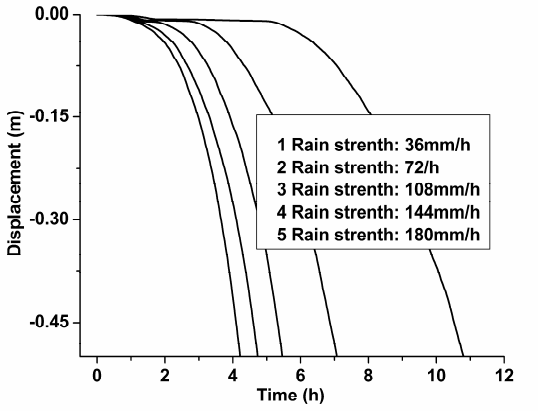

Figure 8 Horizontal developments at point B under different rainfall intensities

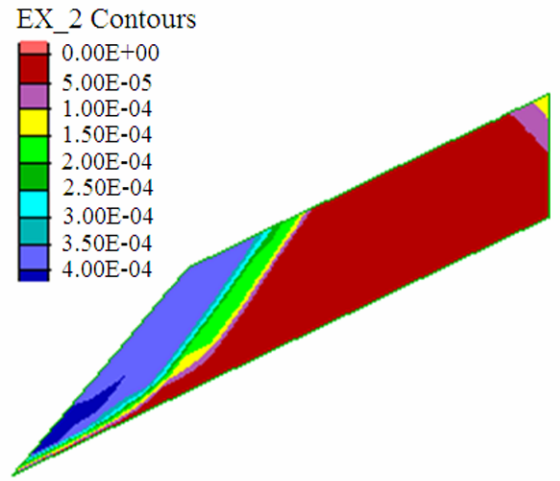

Figure 9 Distribution of displacement at 200s

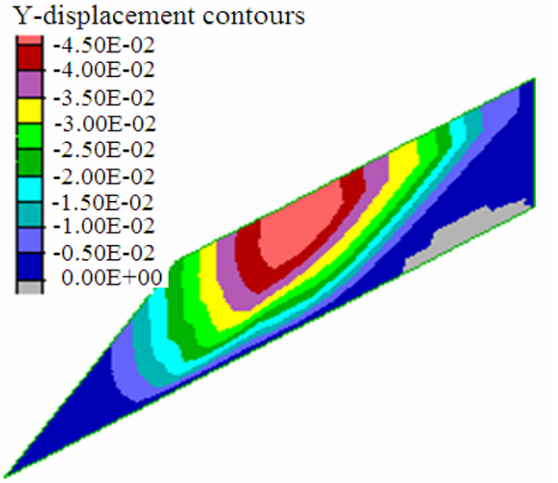

Figure 10 Distribution of vertical displacement

sliding surface (Figure 9). The vertical displacements of the soils decrease from the top to the bottom of the slope (Figure 10). The soil's total velocity vectors showed that the soils (Figure 11) move from the back to the toe of the slope along curved lines. The displacements at point A are chosen to investigate the effects of main factors on the slope's deformation under rainfall. The increase of Yang's modulus and cohesion and internal friction angle cause the decrease of displacement (Figures 12-14). In other words, the stiffness and the strength of the soils limit the development of slope deformation. So, it is an effective method to compact the slope to prevent the occurrence of the landslide and the debris flow.

Figure 15 shows the distribution of the shear stresses in the slope. At the upper part, soils slide downwards the slope toe and the directions of the shear stresses are upwards. The distribution of the shear stresses tends to be non-uniform from nearly layered distributed at the beginning.

Figure 16 shows the distribution of the stresses in the X direction (X-stresses) in the slope. The X-stresses increase from the top to the bottom of the slope. The zero stress area and the tension stress area increase with time under rainfall. Therefore, the unstable area increases with time under rainfall.

Figure 17 shows the distribution of the stresses in the Y direction (Y-stresses) in the slope. It is shown that the Y-stresses increase from the top to the bottom of the slope like the X-stresses. However, the Y-stresses are nearly layered distributed with time under rainfall. It indicates that the rainfall penetrates relatively uniformly into

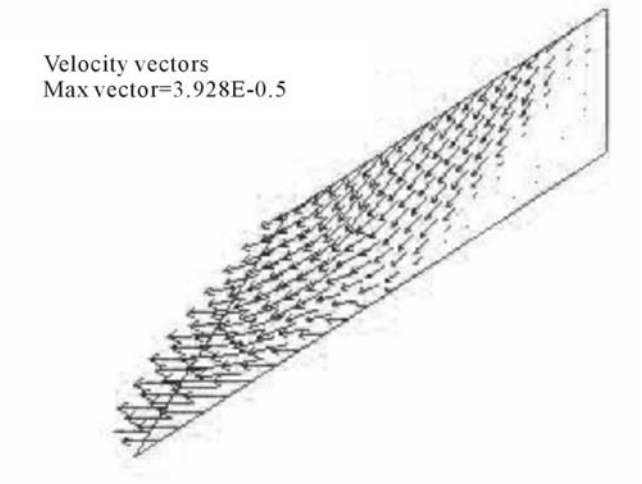

Figure 11 Vector of soil's total velocity $\overline{V}$

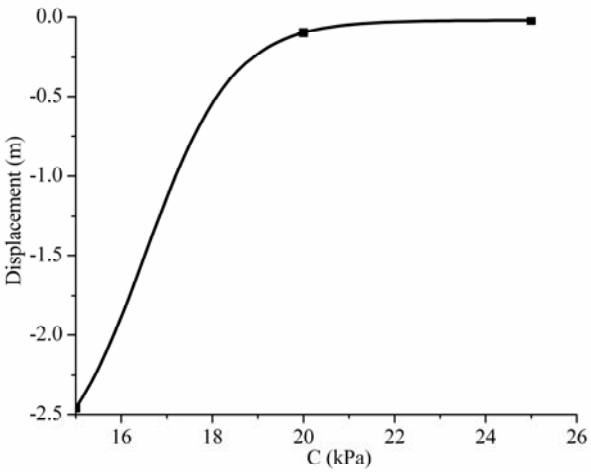

Figure 13 Displacements at point A versus cohesion

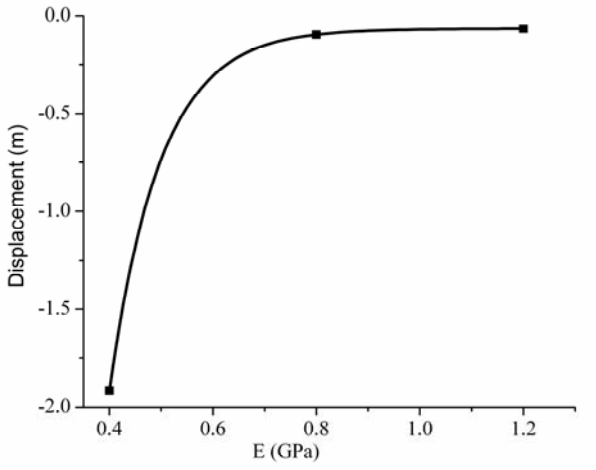

Figure 12 Displacement at point A versus Yang's modulus ($\overline{V} = \overline{V}_x + \overline{V}_y$)

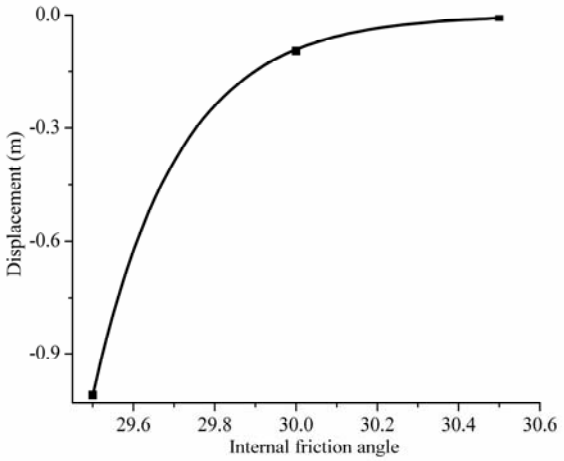

Figure 14 Displacements at point A versus internal friction angle

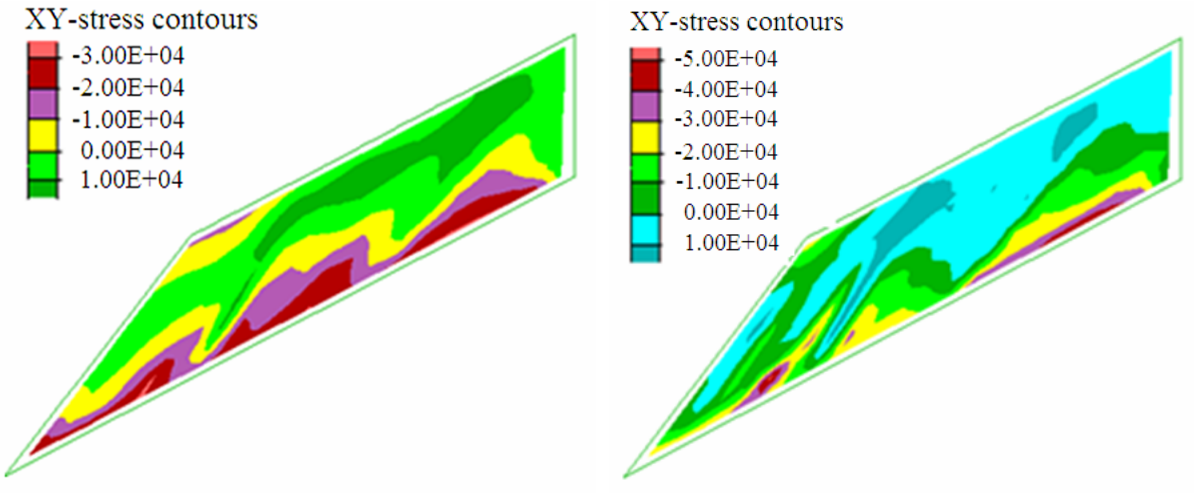

(a) t=100s (b) t=400s

Figure 15 Distribution of shear stress

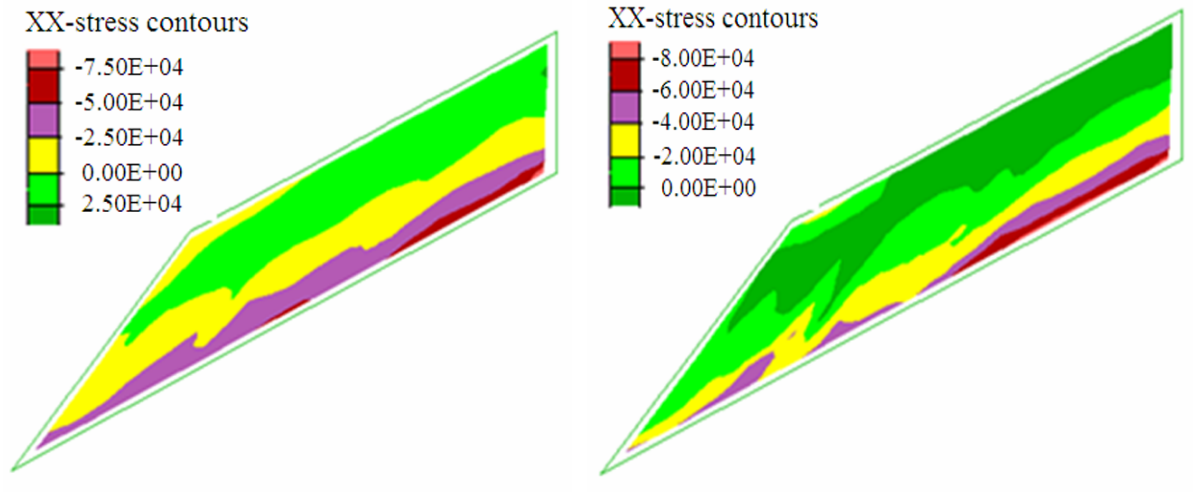

(a) t=100s (b) t=400s

Figure 16 Distribution of stresses in X direction

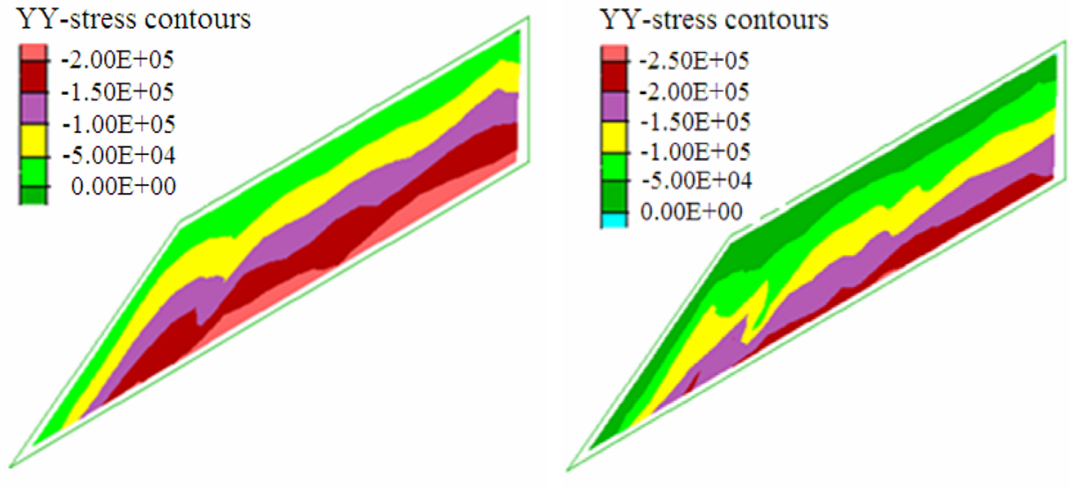

(a) t=100s (b) t=400s

Figure 17 Distribution of stresses in Y direction

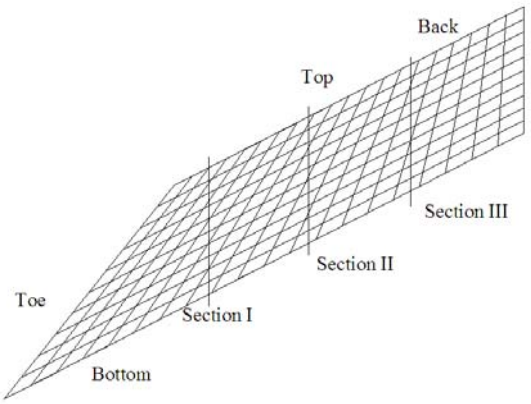

Figure 18 Three referenced sections

the slope in the Y-direction, and meanwhile the settlement is relatively uniform.

Figure 19 shows the distribution of the X-stresses in the three sections of the slope shown in Figure 18. In each section, the X-stresses become from negative to positive at the upper part. From the toe to the back, the X-stresses increase at the upper part. A sliding surface can be traced by connecting the maximum X-stress in different sections.

Figure 20 shows the distribution of the Y-stresses in the three sections of the slope shown in Figure 18. The Y-stresses increase almost linearly from the top to the bottom of the slope in different sections, which is not similar to the X-stresses. It indicates that the deformation of the slope is mainly downwards to the toe.

Figure 21 shows the distribution of the X-stresses in the three sections of the slope shown in Figure 18. It can be found that near the toe, the stresses are negative at the upper part and the lower part, while it is positive at the middle part. It indicates that the sliding points are located in the middle of the slope. At the back of the slope, the distribution of the stresses shows that the sliding points located at the upper part. These points form a sliding surface from the toe to the back.

4 Certification of the Numerical Simulation

To certificate the numerical simulation, some model experiments were carried out in an organic glass trough. The sample of the soil slope was

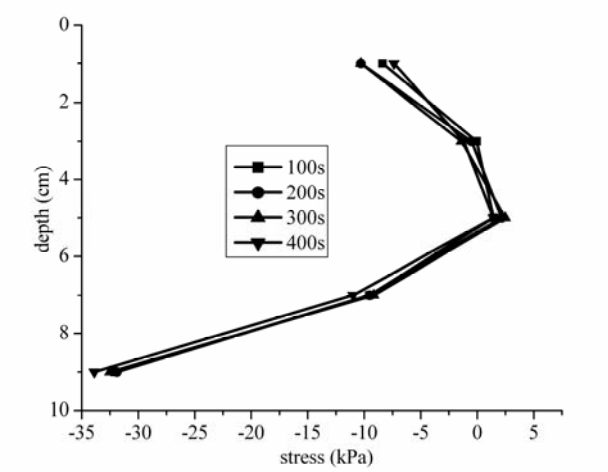

(a)

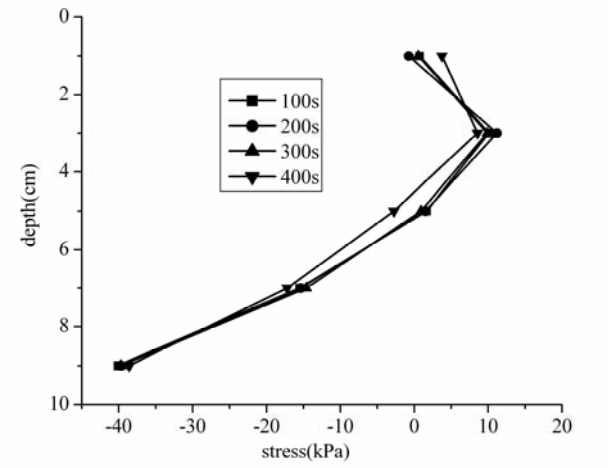

(b)

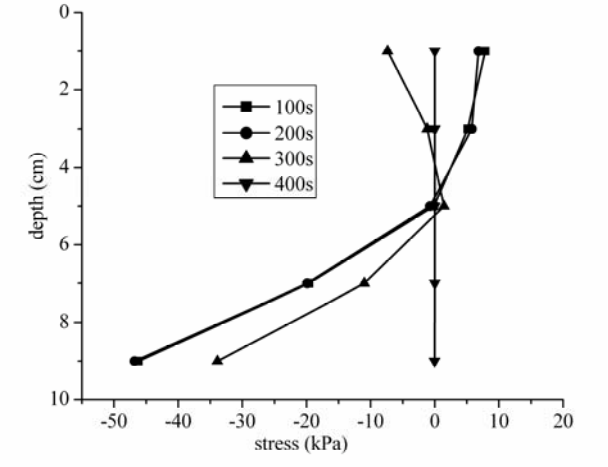

(c)

Figure 19 Distribution of the X-stresses in different sections

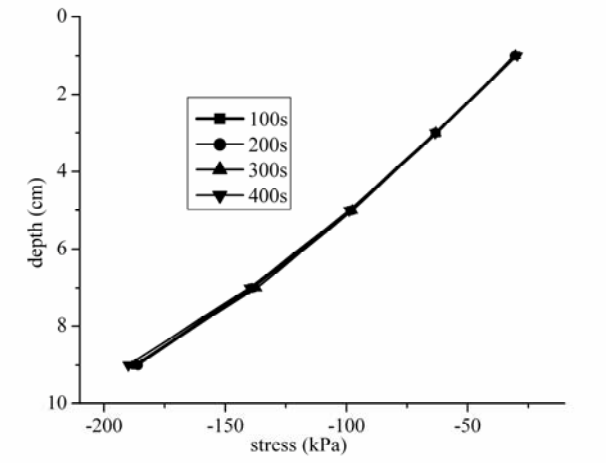

20 (a)

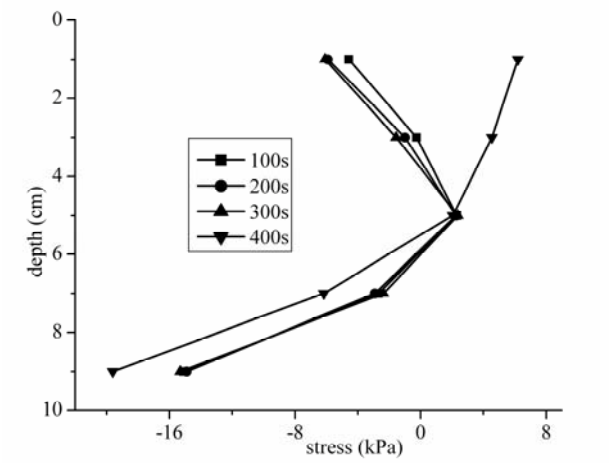

21 (a)

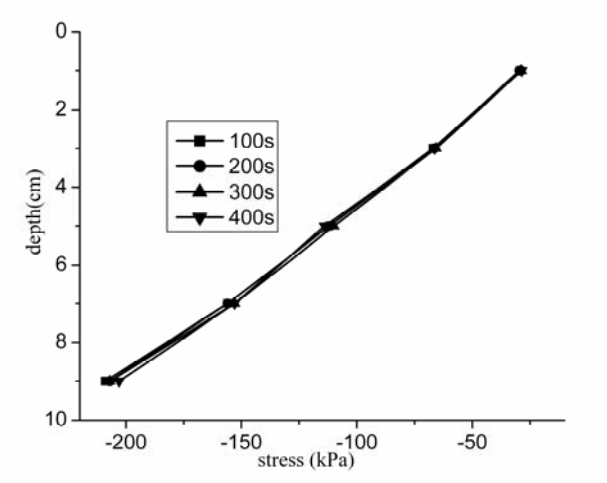

20 (b)

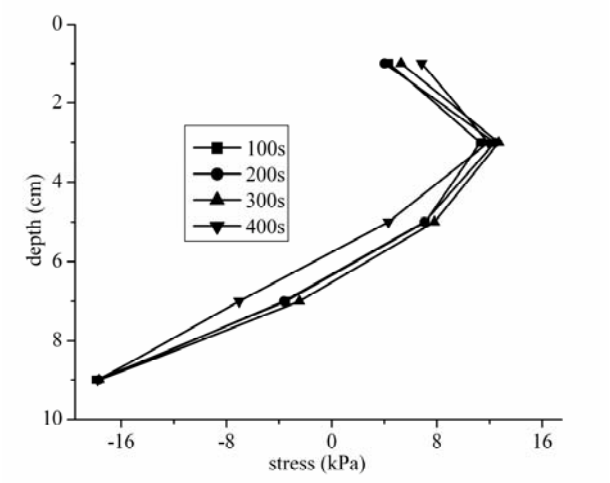

21 (b)

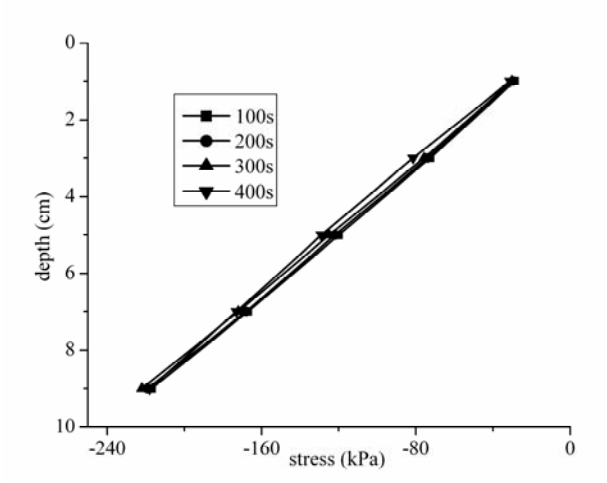

20 (c)

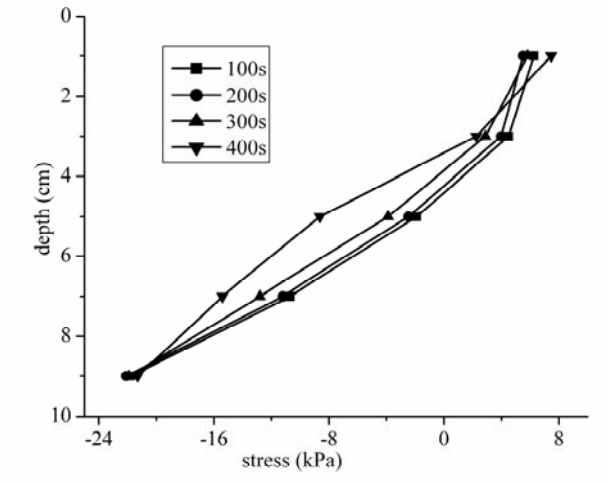

21 (c)

Figure 20 Distribution of the Y-stresses in different sections

Figure 21 Distribution of the shear stresses in different sections

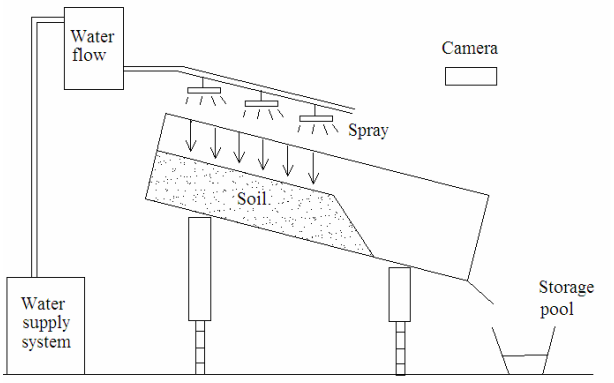

Figure 22 Sketch of the model

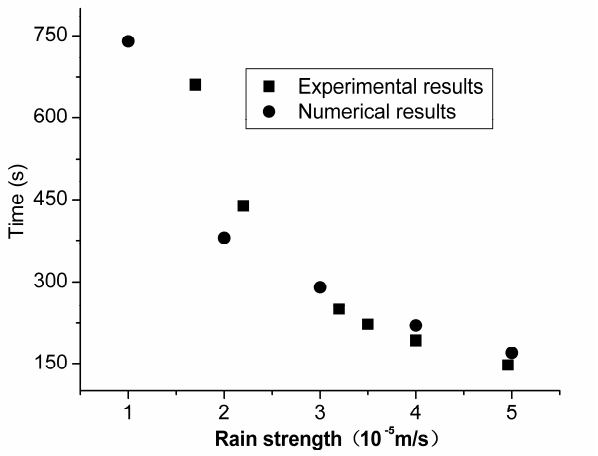

Figure 23 Comparison of the numerical and experimental results

prepared as a trapezia with a size of top × bottom × width × thickness = 35 cm × 52 cm × 21 cm × 10 cm (Figure 22). The slope angles in experiments were 27°, 30°, 32° and 33° respectively considering the in-situ conditions in Weijia Gully. Some water was sprayed on the soil sample to make the soil to have a given water saturation degree after depositing it. For each slope angle, 5 kinds of rainfall intensities were adopted ranging from 36mm/h~180m/h with an interval of 36m/h. During experiments, the displacements of the slope and the duration for debris flow to initiate were recorded.

For any given slope angle, the duration of the rainfall corresponding to the initiation of debris flow decreases with the increase of rainfall intensity (Figure 23). They form an approximate exponential curve. There exists a critical rainfall intensity, less than which no debris flow can initiate. And there exists a critical rain duration, less than which there is no debris flow happens. It can be observed that the displacement of the soil is small and increases slowly before a critical duration corresponding to a rainfall intensity. However, once the rain duration is over the critical duration, the displacement increases very fast, i.e. catastrophic. The numerical results of the rainfall intensity and the rain duration are shown to be close with the experimental results, which indicates that the numerical results are reliable (Figure 23).

5 Conclusions

The responses of the slope during rainfall and the initiation of debris flow were numerically investigated. By compared with the experimental results, the numerical results are certificated to be reliable. The main conclusions are as follows:

(1) The displacements of the slope increase with time and raise fast with the increase of rainfall intensity. The development of the slope's displacements and the pore pressures are catastrophic.

(2) The largest horizontal displacement of the slope is located at the slope toe. The vertical displacements of the slope decrease along depth.

(3) The increase of the Yang's modulus and cohesion and internal friction angle cause the decrease of displacements of the slope.

References

Aleotro P (2004) A warning system for rainfall-induced shallow failures. Engineering Geology 73: 247-265.

Chen XQ, Cui P, Feng ZL et al. (2006) Artificial rainfall experimental study on landslide translation to debris flow. Chinese Journal of Rock Mechaics & Engineering 25(1): 106-116. (In Chinese)

Cui Peng, Liu SQ, Tang BX et al. (2003) Debris flow prevention pattern in national parks-Taking the world natural heritage Jiuzhaigou as an example. Science in China Series E-Engineering. & Material Science 46(suppl.): 1-11. (In Chinese)

Cui P, Ge YG, Zhuang JQ, et al. (2009) Soil evolution features of debris flow waste-shoal land. Journal of Mountain science

6(2): 181-188.
Cui P, Liu SJ, Tan WP. (2000) Progress of debris flow forecast in China. Journal of Natural disasters 9(2): 10-15. (In Chinese)
Cui P (1992) Study on condition and mechanisms of debris flow initiation by means of experiment. Chinese Science Bulletin 37(9): 759-763. (In Chinese)
Chen CY, Chen TC, Yu FC, et al. (2005) Rainfall duration and debris-flow initiated studies for real-time monitoring. Environment Geology 47: 715-724.
Iverson RM, Reid ME, LaHusen RG. (1997) Debris-flow Mobilization from landslides, Annual Review of t Earth and Planet. Science 25:85-138.
Lu XB, Zheng ZM. (2006) Formation of water film in saturated sand. ACTA Mech. Sinica 22: 377-383.
Lu XB, Cui P (2010) On the study of water film in saturated soils. International Journal of Sediment Research 25: 221-232.
Lu XB, Cui P, Hu KH et al. (2010) The initiation and development of water film by seepage. Journal of Mountain Science, 7: 361-366
Reid ME, LaHusen RG, Iverson RM. (1997) Debris-flow initiation experiments using diverse hydrologic triggers. In: Cheng-Lung Chen, (eds.) Debris-flow hazards mitigation: Mechanics, Prediction, and Assessment. ASCE 1-11.
Wu LZ, Zhang LM (2009) Analytical solution to 1D coupled water infiltration and deformation in unsaturated soils. International Journal of Numerical and Analytical Methods in Geomechanis 33(6): 773-790.
Ye TL (2011) Study of the Initiation of Debris Flow after Strong Earthquake, Thesis for Master Degree, Institute of Mechanics, Chinese Academy of Sciences, Beijing.
Zhang LL, Zhang LM and Tang WH (2005) Rainfall-induced slope failure considering variability of soil properties. Geotechnique 55(2): 183-188.